

RESEARCH ARTICLE

Biomechanical and tomographic differences in the microarchitecture and strength of trabecular and cortical bone in the early stage of male osteoporosis

Poh-Shiow Yeh^{1,2}, Yuan-Wen Lee^{3,4}, Wei-Hui Chang², Weu Wang⁵, Jaw-Lin Wang⁶, Shing-Hwa Liu⁷, Ruei-Ming Chen^{2,4,8*}

1 Department of Neurology, Chi Mei Medical Center, Tainan, Taiwan, **2** Graduate Institute of Medical Sciences, College of Medicine, Taipei Medical University, Taipei, Taiwan, **3** Department of Anesthesiology, School of Medicine, College of Medicine, Taipei Medical University, Taipei, Taiwan, **4** Anesthesiology and Health Policy Research Center and Department of Anesthesiology, Taipei Medical University Hospital, Taipei, Taiwan, **5** Division of General Surgery, Department of Surgery, Taipei Medical University Hospital, Taipei, Taiwan, **6** Institute of Biomedical Engineering, National Taiwan University, Taipei, Taiwan, **7** Institute of Toxicology, College of Medicine, National Taiwan University, Taipei, Taiwan, **8** Cell Physiology and Molecular Image Research Center, Wan Fang Hospital, Taipei Medical University, Taipei, Taiwan

☯ These authors contributed equally to this work.

* rmchen@tmu.edu.tw



OPEN ACCESS

Citation: Yeh P-S, Lee Y-W, Chang W-H, Wang W, Wang J-L, Liu S-H, et al. (2019) Biomechanical and tomographic differences in the microarchitecture and strength of trabecular and cortical bone in the early stage of male osteoporosis. *PLoS ONE* 14(8): e0219718. <https://doi.org/10.1371/journal.pone.0219718>

Editor: Joseph M. Wallace, Indiana University Purdue University at Indianapolis, UNITED STATES

Received: April 18, 2019

Accepted: June 28, 2019

Published: August 8, 2019

Copyright: © 2019 Yeh et al. This is an open access article distributed under the terms of the [Creative Commons Attribution License](https://creativecommons.org/licenses/by/4.0/), which permits unrestricted use, distribution, and reproduction in any medium, provided the original author and source are credited.

Data Availability Statement: All relevant data are within the paper and its Supporting Information files.

Funding: This study was supported by grants from the Chi-Mei Medical Center (102CM-TMU-14-4), Wan Fang Hospital (108-wf-eva-04), and the Ministry of Science and Technology (MOST107-2314-B-038-036-MY3), Taipei, Taiwan.

Competing interests: The authors have declared that no competing interests exist.

Abstract

Osteoporosis is a continuous process of loss of bone tissue. Compared to women, osteoporosis in men is associated with greater morbidity and mortality. In this study, we conducted tomographic and biomechanical evaluations of trabecular and cortical bone in the early stage of male osteoporosis. Male Wistar rats were subjected to orchietomy and sham operation. Four weeks after being castrated, decreased levels of testosterone in plasma were found and resulted in concurrent bone loss. Separately, the orchietomy led to significant tomographic alterations in the trabecular bone number, trabecular separation, and trabecular pattern factor. Data of a mechanistic compression test further showed that the orchietomy diminished the maximum loading force, displacement at maximum load, energy at maximum load, and ultimate stress. Interestingly, orchietomy-triggered changes in the maximum loading force and tomographic parameters were highly correlated. In contrast, tomographic and biomechanical analyses showed that 4 weeks after rats were orchietomized, the thickness, area, maximum loading force, bone stiffness, energy at maximum load, and ultimate stress of the cortical bone were not changed. Taken together, this study showed specific differences in the microarchitecture and strength of trabecular bone in the early stage of male osteoporosis.

Introduction

Osteoporosis, a systemic aging skeletal disorder, is characterized by increased bone fragility and high risks of bone fracture [1, 2]. According to a report by the World Health Organization,

osteoporosis is one of the most common metabolic diseases in the world [3]. Thus, osteoporosis is a public and critical healthcare issue now and in the future. Multiple risk factors are involved in the incidence of osteoporosis, including age, genetics, hormonal variations, smoking, and calcium and vitamin D deficiencies [4]. In the past, osteoporosis was generally considered to be a woman's disease, because men have larger skeletons, bone loss starts later and advances more slowly, and there was no period of rapid hormonal change [5, 6]. Recently, osteoporosis in men has been a focus of researchers, healthcare professionals, and clinicians [7]. Compared to women, osteoporosis in men exhibits different pathophysiological stages. Riggs et al. showed that loss of cortical bone begins after the age of 75 years in men [8]. In women, loss of cortical bone occurs much earlier [9]. According to a statistical report by the National Osteoporosis Foundation, men experience 42% of total lifetime trabecular bone loss before the age of 50 years [5]. In women, trabecular bone is lost with age, and such a bone injury is accelerated during perimenopause [10]. Nevertheless, older men are more likely to become osteoporotic with a total testosterone deficiency [11, 12]. As a result, osteoporosis in men and women has noteworthy variances in pathophysiology and clinical risks.

Bone loss in men commonly comes about later in life. A variety of hazard factors such as chronic diseases, lifestyle habits, medication use, male sex hormones, calcium intake, heredity, and aging contribute to causes of osteoporosis in men [13]. Among these factors, the sex hormones, androgens, play crucial roles in regulating bone remodeling and maintaining the bone mass [14]. In particular, testosterone has the highest concentration and mainly controls the development and maintenance of masculine physiognomy [12, 15]. Levels of blood androgens decrease with aging, and an androgen deficiency is recognized as the main cause of osteoporosis in men [14, 16]. In elderly men, preserving ideal levels of androgens is essential to preventing osteoporosis and its complications [12]. In addition, bone fractures are major complication of osteoporotic patients [17]. Prominently, osteoporosis in men has a higher mortality rate due to hip, vertebral, and other major fractures [18, 19]. High morbidity and mortality of osteoporosis-connected fractures impose heavy economic burdens on patients, their families, and society.

Dual-energy x-ray absorptiometry (DXA), micro-computed tomography (μ CT), and peripheral quantitative computed tomography (pQCT) are widely used and powerful tools for analyses of bone geometry and densitometry [20]. These radiographic methodologies can evaluate the bone architecture and bone mass by measuring x-ray absorptiometry of mineral tissues [20, 21]. In the clinic, DXA is a standard approach to assess bone mineral density (BMD) through scanning and recording the mineral absorption content of the target site. Nevertheless, previous studies showed that BMD cannot completely and accurately reflect the risk of osteoporosis-associated bone fractures [21–23]. Especially in elderly men, only 21% of non-vertebral fracture patients were detected as having osteoporosis, defined as a BMD of < -2.5 . Thus, analysis of BMD is insufficient to elucidate the bone strength and fracture risk [22]. Biomechanical approaches can provide alternative methodologies for assessing bone strength and osteoporosis-associated fracture risks. Mechanistic reduced-platen compression (RPC) and four-point bending (FPB) tests can be applied to measure the strength of trabecular and cortical bone [24, 25]. Ovariectomy and orchietomy are two typical surgical techniques for induction of bone loss in female and male rodents, respectively [26]. Our previous study showed that ovariectomy led to a significant reduction in levels of serum estrogen and a consequent loss of bone mass in female rats [27]. In comparison, orchietomy can induce testosterone deficiency and bone loss in male animals via the receptor activator of nuclear factor kappa β -ligand (RANKL)-osteoprotegerin (OPG) signaling pathway [26, 28, 29]. In this study, we used tomographic and biomechanical approaches to evaluate differences in the microarchitecture and strength of trabecular and cortical bone in the early stage of male osteoporosis using

orchiectomy rats as the experimental model. We hypothesize that orchiectomy can cause associated declines in the microarchitecture and strength of trabecular and cortical bone in the early stage of osteoporosis in rats.

Material and methods

Animals

Male Wistar rats (250~300 g) purchased from BioLASCO (Taipei, Taiwan) were housed in an environmentally controlled room, with a standard 12-h light/dark cycle and free access to laboratory chow (Teklad Global Diets, Indianapolis, IN, USA) and tap water. All procedures were performed according to the National Institutes of Health *Guidelines for the Use of Laboratory Animals* and were approved by the Institutional Animal Care and Use Committee of Taipei Medical University-Wan Fang Hospital, Taipei, Taiwan (Approval no. WAN-LAC-103-008). Animals were randomly allocated into sham-operated and orchiectomy groups. Each assay was repeated for more than 3 times (3 independent determinations). There were at least 3 animals per group for every determination. Total number of animals used in this study was more than 20 rats.

Orchiectomy

Orchiectomy was conducted using a castration rat model as described previously [30]. All surgical procedures were performed under sterile conditions and general anesthesia, which was comprised of inhalation of 1%~2% isoflurane. For the orchiectomy, a 10-mm incision was made in the skin of the lower abdomen over one testis of a rat. The testis and associated fat pad were pulled with forceps. The connective tissues leading to the testis which included the fat pad, testicular vein, and vas deferens were tied using surgical silk. Connective tissues between the testis and knot around the connective tissue were cut. Finally, the connective tissues were returned to the body cavity. The wound was cleaned and sutured. In the sham group, animals received a 3-cm wound, which was immediately stitched closed. Four weeks after surgery, rats were euthanized via terminal bleeding under isoflurane-anesthesia, and femurs and tibias were collected. Following the removal of adherent soft tissues, bone tissues were washed with phosphate-buffered saline (PBS, 0.14 M NaCl, 2.6 mM KCl, 8 mM Na₂HPO₄, and 1.5 mM KH₂PO₄).

Quantification of plasma testosterone

Levels of plasma testosterone were quantified according to a previous method [31]. After surgery for 4 weeks, blood was collected from a tail vein of rats. Following centrifugation, the plasma fraction was prepared. Testosterone in plasma was extracted with diethyl ether. The organic phase was evaporated to dryness. Levels of plasma testosterone were measured with a colorimetric competitive enzyme immunoassay kit (Enzo Life Sciences, Farmingdale, NY, USA). Results were read on a colorimetric plate reader (BioTek, Vermont, FL, USA) at 405 nm.

Analysis of μ CT

The bone volume and architecture were evaluated using μ CT as described previously [32]. The μ CT analysis was conducted using a Skyscan 1176 scanner (Bruker, Billerica, MA, USA). The scanning axis nominally coincided with the diaphyseal axis of the control femur. Femurs with a bone defect were scanned using the same parameters (9 μ m per slice, 65 kV, 385 μ A, 1-mm Al filter, and a 3300-ms exposure time). High-resolution images of the femurs were

generated for 3D polygonal resampling using Skyscan 3D-Creator software (Bruker), and morphometric parameters, including the trabecular number (Tb.N.), trabecular separation (Tb.Sp.), and trabecular thickness (Tb.Th.), were calculated for trabecular bone regions of interest (ROIs) using a Skyscan CT-Analyzer (vers. 1.10, Bruker) as described previously [33]. In addition, the cortical bone area, total area ratio, and cortical bone/total area ratio were analyzed as cortical architectural parameters.

Test of reduced-platen compression (RPC)

The RPC test was performed according to a modified protocol following a previously described method [34]. Prior to this mechanical test, tibia specimens from the sham and orchietomized groups were immersed in 0.9% saline solution for 2 h for rehydration. The upper part of the cortical shell was removed in order to expose the trabecular region of the tibia. The size of the platen was reduced to 2 mm in diameter, and the tibia specimen was aligned such that contact was only made with cancellous bone (Fig 1A). An extensometer (Model 5500, Bose, Framingham, MA, USA) was applied to compress the tibia specimen for 2 mm in depth in the central part. The rate of displacement was 0.5 mm/min. The load and displacement were recorded every 10 ms. The cross-sectional area (CSA) was the area of the reduced platen (3.14 mm²). The maximum loading force was divided by the CSA to calculate the ultimate stress (σ_{\max}) (Fig 1D).

Test of four-point bending (FPB)

The FPB test was conducted following a modified protocol described previously [35]. Prior to the mechanistic test, a femur was thawed at room temperature and then rehydrated in a 0.9% saline solution for 2 h. An extensometer (Bose) was used to compress the femur specimen for analysis of material resistance and deformation behavior. This apparatus was built of two major parts, the upper loading arms and the lower supporting arms (Fig 1B). The lengths of the upper and lower arms were 10 and 20 mm, respectively. The rate of displacement was 0.5 mm/min. Femur specimens were compressed to 2 mm or until fracture. The load and displacement were recorded every 10 ms. The area moment of inertia (I) was calculated according to the formula shown in Fig 1D as described previously [36]. Considering the hollow structure of the diaphysis, values of α , α' , β , and β' in the formula were analyzed by μ CT images and used to calculate I. Then, the ultimate stress (σ_{\max}) was calculated according to the formula in Fig 1D. In that formula, F is the maximum load, and L_a is the moment arm in the FPB test.

Statistical analysis

The statistical significance of differences between groups was evaluated using a one-way analysis of variance (ANOVA) with Duncan's multiple-range test. Differences were considered statistically significant at p values of < 0.05 . Correlations between tomographic and biomechanical differences in the trabecular bone and cortical bone were evaluated by a linear regression analysis. The r value of a linear regression was calculated in order to present the association of those two parameters.

Results

Orchiectomy caused significant decreases in testosterone levels

Levels of plasma testosterone in untreated animals were detected (Fig 2). In contrast, at 4 weeks after the orchietomy, male Wistar rats exhibited a 57% reduction in levels of plasma testosterone compared to the sham group ($p = 0.0002$).

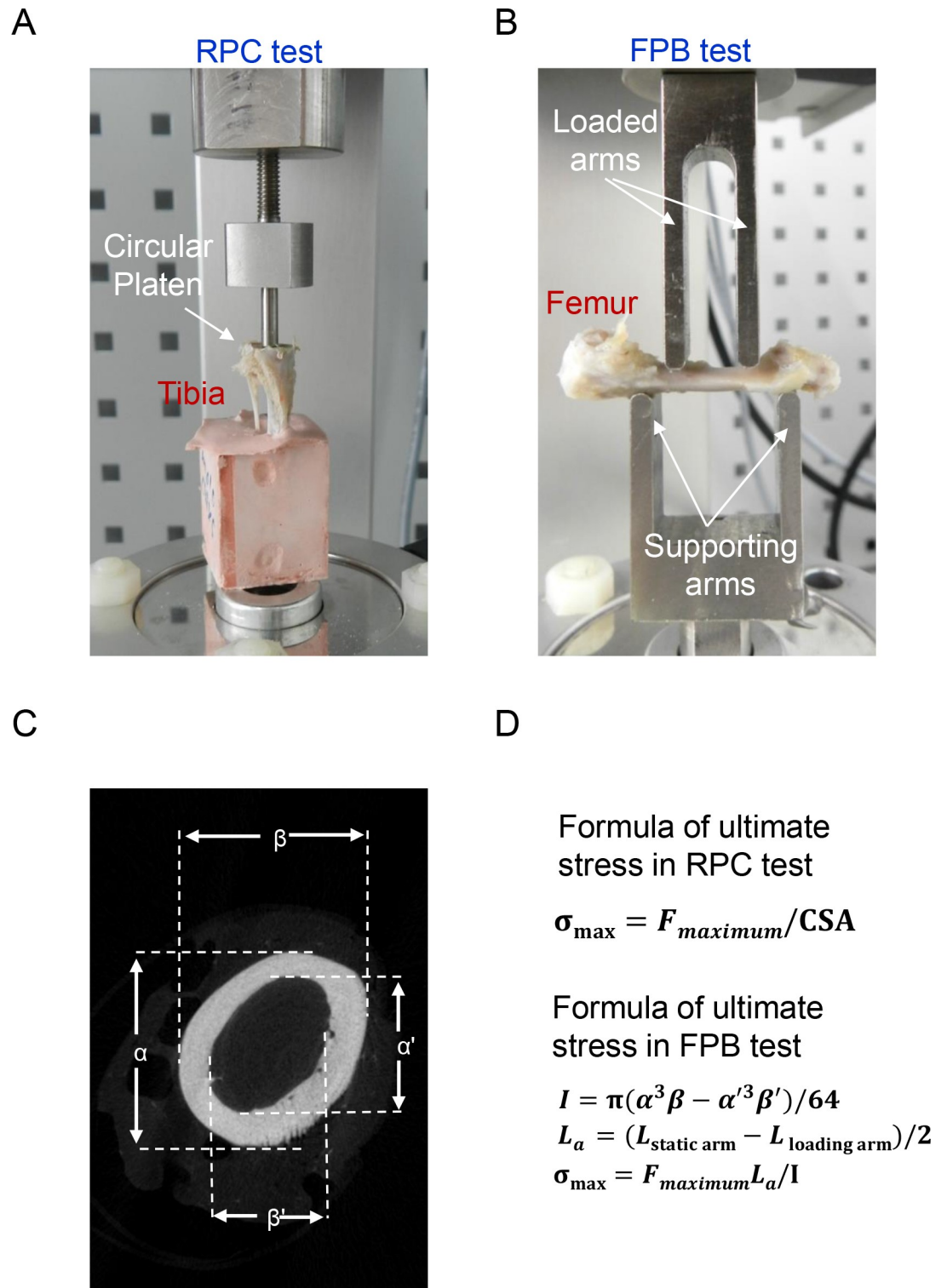


Fig 1. Biomechanical and tomographic methodologies. Male Wistar rats were subjected to sham operation or orchietomy. After sacrifice, tibias and femurs from sham and orchietomized rats were collected for analyses of mechanistic reduced-platen compression (RPC) and four-point bending (FPB) (A and B) as well as micro-computed tomography (μ CT) (C). In the RPC test, the upper cortical shell of a tibia was removed in order to expose the trabecular region. The strength of trabecular bone was measured using a circular platen to compress the trabecular bone (A). In the FPB test, a femur was placed across two supporting arms and compressed by double loaded arms with a constant force until the specimen broke (B). The external (α and β) and

internal (α' and β') diameters of the femur were measured by μ CT in order to calculate the cross-sectional area (CSA) (C). The ultimate stress (σ_{\max}) in the RPC and FPB tests were calculated according to two different formulas (D). F_{\max} , maximum force during loading history; I , area of inertia; L_{α} , distance between the supporting and loading pins; $L_{\text{loading arm}}$, length of the loading span; $L_{\text{static arm}}$, length of the supporting span.

<https://doi.org/10.1371/journal.pone.0219718.g001>

Analyses of tomographic parameters revealed loss of trabecular bone in orchietomized rats

Representative tomographic images from scanning femurs using μ CT showed that at 4 weeks after the orchietomy, an obvious decrease in the bone volume and an increase in bone porosity had been induced (Fig 3A). Compared to sham animals, 4 weeks after being castrated, rats showed a significant 25% reduction in the trabecular bone number ($p = 0.0038$) (Fig 3B). At the same time, the orchietomy caused a decrease in the separation of trabecular bone by 18% compared to sham rats ($p = 0.021$) (Fig 3C). Afterward, the trabecular pattern factor was meaningfully augmented by 93% ($p = 0.0018$) at 4 weeks following the orchietomy (Fig 3D). In contrast, the trabecular thickness between sham and orchietomized animals was not influenced ($p = 0.8512$) (Fig 3E).

Mechanistic analyses by an RPC test further demonstrated the suppressive effects of orchietomy on the strength of trabecular bone

In the sham group, a load-displacement curve displayed a maximum loading force to break trabecular bone of 105 N at a displacement of 0.64 mm (Fig 4A). In comparison, 4 weeks after being castrated, the maximum loading force to break trabecular bone of an orchietomized rat was reduced to 58 N at a displacement of 0.33 mm. In addition, compared to sham rats, the load-displacement curve in orchietomized animals had obviously shifted (Fig 4A). After

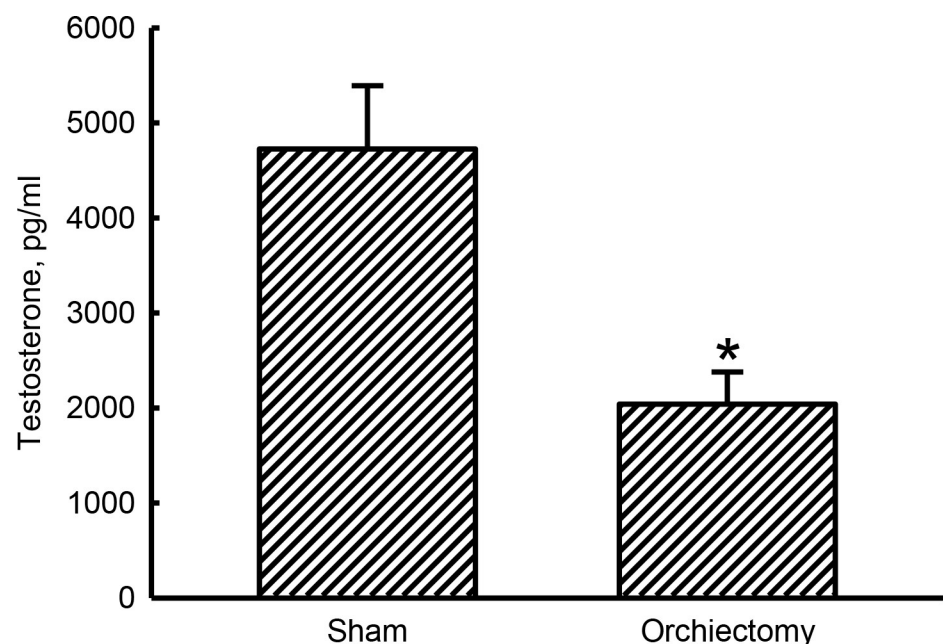


Fig 2. Effects of orchietomy on reductions in testosterone levels. Male Wistar rats were subjected to sham operation or orchietomy. Four weeks after surgery, blood samples were collected for analysis of plasma testosterone using an enzyme-linked immunosorbent assay. Each value represents the mean \pm SD of three independent determinations. * Indicates that the value significantly ($p < 0.05$) differed from the sham group.

<https://doi.org/10.1371/journal.pone.0219718.g002>

being orchietomized, the maximum loading force was diminished by 44% ($p = 0.0012$) (Fig 4B). In contrast, castration led to a 37% drop in the displacement at the maximum load compared to control animals ($p = 0.0045$) (Fig 4C). Fascinatingly, the energy at maximum load to

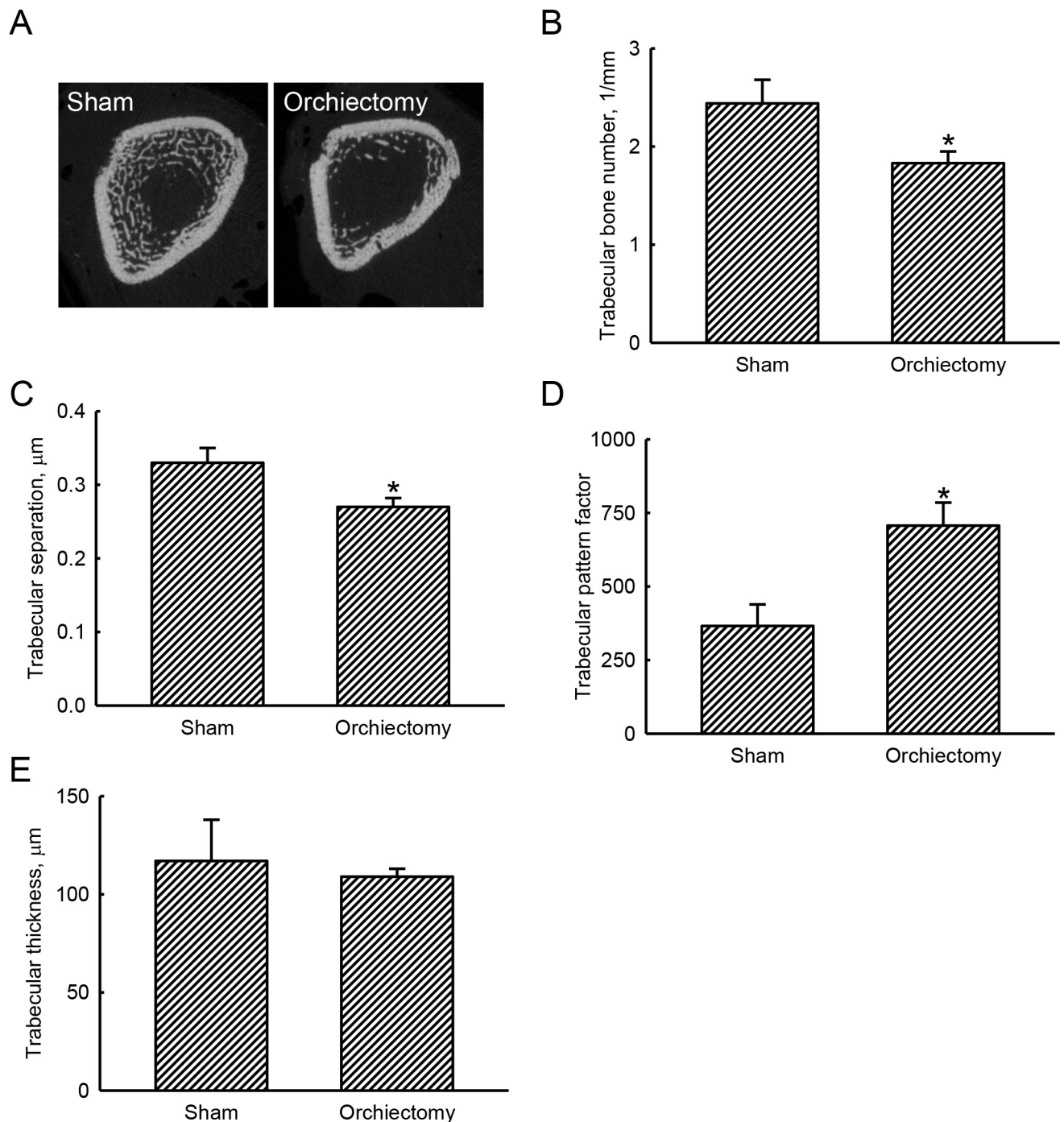


Fig 3. Effects of orchietomy on tomographic changes of trabecular bone. Male Wistar rats were subjected to sham operation or orchietomy. Four weeks after surgery, animals from the sham and orchietomy groups were sacrificed, and their femurs were collected for analysis by micro-computed tomography ($\mu\text{-CT}$). The distal femur was scanned with $\mu\text{-CT}$, and representative cross-sectional images are presented (A). Tomographic parameters, including the trabecular bone number (B), trabecular separation (C), trabecular pattern factor (D), and trabecular thickness (E), were examined and statistically analyzed. Each value represents the mean \pm SD of three independent determinations. * Indicates that the value significantly ($p < 0.05$) differed from the sham group.

<https://doi.org/10.1371/journal.pone.0219718.g003>

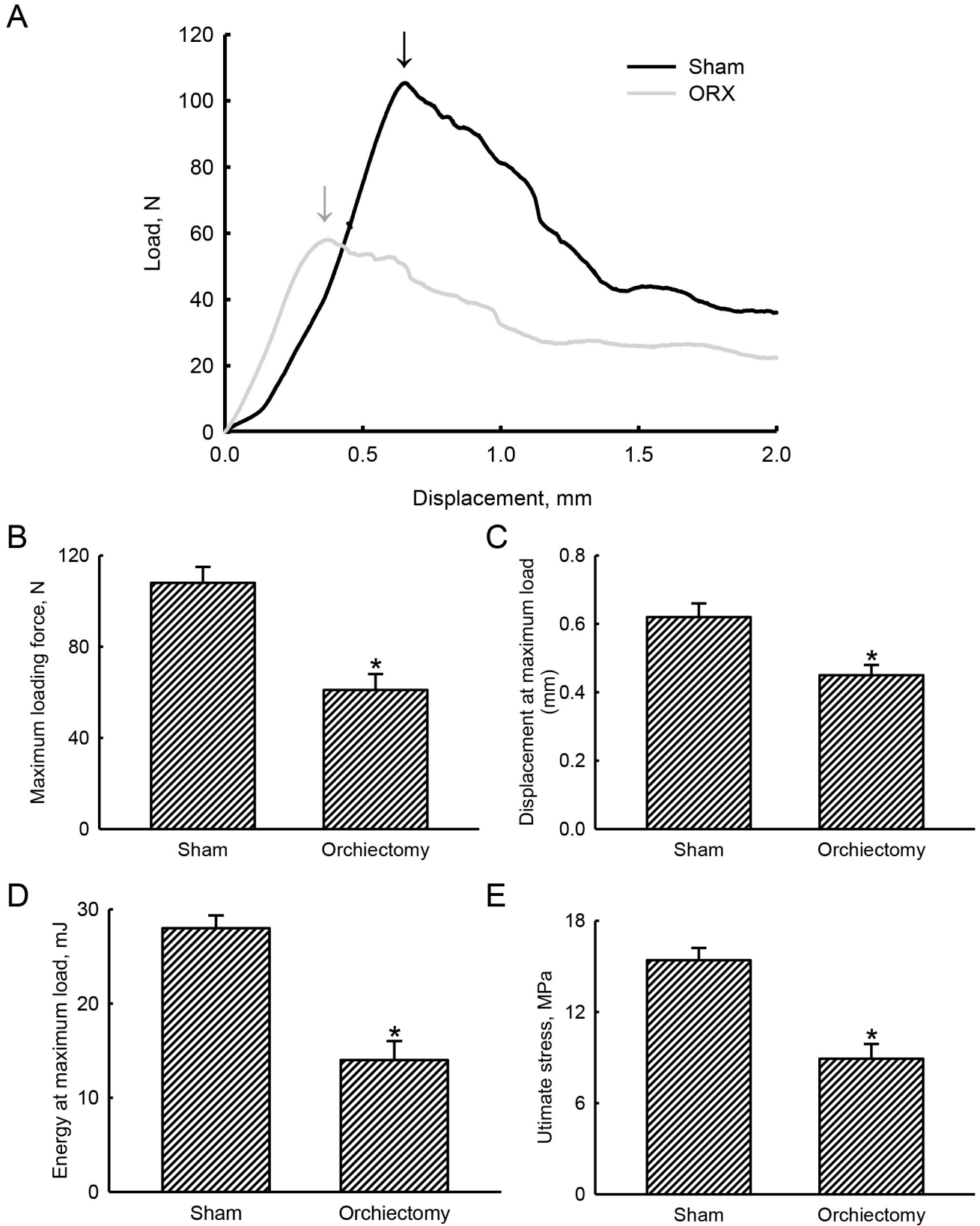


Fig 4. Effects of orchiectomy on biomechanical changes of trabecular bone. Male Wistar rats were subjected to sham operation or orchiectomy. Four weeks after surgery, animals from the sham and orchiectomy groups were sacrificed, and their tibias were collected for analysis of a reduced-platen-compression test. The upper cortical shell of a tibia was removed to expose the trabecular region. A reduced-area platen was used to compress the central area of trabecular bone in the proximal tibia. The compression load and displacement of the tibia were recorded. Representative load-displacement curves in sham and orchiectomized rats are presented (A). Arrows indicate the maximum loading force. Values of these mechanistic parameters, including the maximum loading force (B), displacement at the maximum load (C), energy at the maximum load (D), and ultimate stress (E), were calculated and statistically analyzed. Each value represents the mean \pm SD of three independent determinations * Indicates that the value significantly ($p < 0.05$) differed from the sham group.

<https://doi.org/10.1371/journal.pone.0219718.g004>

break trabecular bone of sham rats was 28.0 ± 1.4 mJ (Fig 4D). However, the energy at the maximum load to break trabecular bone of orchiectomized rats was reduced by 50% ($p = 0.0029$). Consequently, compared to the sham group, the orchiectomy caused a 42% decrease in the ultimate stress ($p = 0.0011$) (Fig 4E).

The effects of orchiectomy were additionally confirmed with correlational analyses of our tomographic and biomechanical data

The castration-induced tomographic decrease in the trabecular bone number was highly correlated with the orchiectomy-induced reduction in the maximum loading force that could break trabecular bone ($r = 0.91$, $p < 0.05$) (Fig 5A). In addition, the tomographic parameters of trabecular separation ($r = 0.83$, $p < 0.05$) and trabecular pattern factor ($r = 0.86$, $p < 0.05$) were exceptionally associated with the maximum loading force in orchiectomized rats (Fig 5B and 5C). However, the tomographic trabecular thickness was not correlated with the biomechanical maximum loading force in the early stage of male osteoporosis ($r = 0.16$, $p = 0.44$) (Fig 5D).

Orchiectomy did not change tomographic architecture and biomechanical strength of cortical bone

Effects of orchiectomy on tomographic changes in the architecture of cortical bone were determined (Table 1). Four weeks after being castrated, the thickness of cortical bone in male Wistar rats was not affected ($p > 0.05$). In addition, the cortical bone area and total bone section area were not influenced at 4 weeks after the orchiectomy ($p > 0.05$) (Table 1). Consequently, the ratio of the cortical bone area over total bone section area did not change in orchiectomized rats ($p > 0.05$) (Table 1).

Biomechanical analyses using an FBP test were performed in order to determine the effects of orchiectomy on the strength of cortical bone (Table 2). At 4 weeks after being castrated, the biomechanical maximum loading force and displacement at the maximum load of cortical bone were not affected ($p > 0.05$). In orchiectomized rats, the biomechanical stiffness and energy at the maximum load did not change ($p > 0.05$) compared to sham animals (Table 2). Moreover, orchiectomy in male rats did not influence the biomechanical ultimate stress ($p > 0.05$) (Table 2).

Correlations of the biomechanical maximum loading force with tomographic parameters in cortical bone were examined (Fig 6). In orchiectomized rats, the tomographic cortical bone area was not significantly correlated with the biomechanical maximum loading force in cortical bone ($r = 0.66$, $p = 0.15$) (Fig 6A). The ratio of the cortical bone area over total bone section area also showed a medium association with the biomechanical maximum loading force ($r = 0.47$, $p = 0.34$) (Fig 6B).

Discussion

The present study provides tomographic and biomechanical evidence to show noteworthy differences in the microarchitecture and strength of trabecular bone in the early stage of male

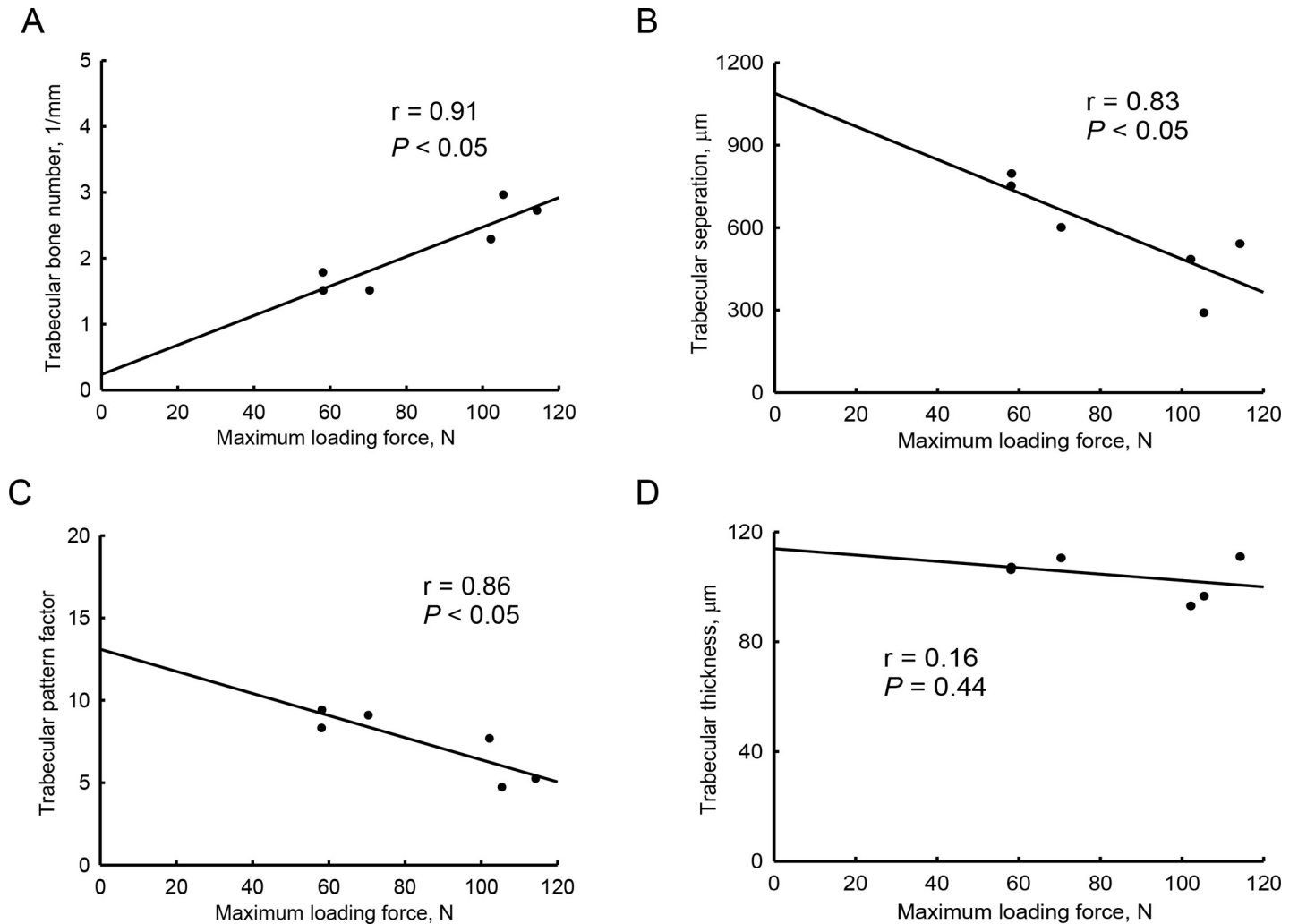


Fig 5. Correlations of the biomechanical maximum loading force with tomographic parameters in orchietomy-treated trabecular bone. Trabecular bones from sham-operated and orchietomized rats were analyzed using micro-computed tomography and a reduced-platen compression test. The trabecular bone number, trabecular separation, trabecular pattern factor, trabecular thickness, and maximum loading force were measured. Correlations of the maximum load force with trabecular bone number (A), trabecular separation (B), trabecular pattern factor (C), and trabecular thickness (D) were analyzed using linear regressions.

<https://doi.org/10.1371/journal.pone.0219718.g005>

Table 1. Tomographic analyses of cortical bone.

	Sham	Orchietomy
Cortical bone thickness (mm)	0.313 ± 0.014	0.326 ± 0.019
Cortical bone area (mm ²)	7.022 ± 0.170	6.948 ± 0.214
Total bone section area (mm ²)	8.200 ± 0.343	8.052 ± 0.265
Ratio of cortical area/total section area (%)	85.90 ± 0.02	86.40 ± 0.02

Male Wistar rats were subjected to sham operation or orchietomy. Four weeks after surgery, animals were sacrificed, and their femurs were collected. These cortical bones were scanned using μ CT. The cortical bone thickness, cortical bone area, and total bone section area were quantified. The ratio of cortical bone area over total bone section area were calculated. Each value represents the mean \pm SD of three independent determinations.

<https://doi.org/10.1371/journal.pone.0219718.t001>

Table 2. Mechanical analysis of cortical bone.

	Sham	ORX
Maximum loading force (N)	177 ± 12	178 ± 8
Displacement at maximum load (mm)	0.85 ± 0.29	0.86 ± 0.29
Bone stiffness (N/mm)	248 ± 63	225 ± 34
Energy at maximum load (mJ)	79 ± 23	91 ± 26
Ultimate stress (MPa)	74 ± 9	86 ± 9

Male Wistar rats were subjected to sham operation or orchietomy (ORX). Four weeks after surgery, animals were sacrificed, and their femurs were collected. Mechanical analyses of these cortical bones were carried out using a four-point-bending test. The maximum force, displacement at the maximum force, stiffness, energy of the maximum force, and ultimate stress were calculated and statistically analyzed. Each value represents the mean ± SD of three independent determinations.

<https://doi.org/10.1371/journal.pone.0219718.t002>

osteoporosis. Orchietomy is a valuable experimental model for research of osteoporosis and osteoporotic fractures [30]. This study showed that levels of testosterone in plasma of male Wistar rats were meaningfully decreased at 4 weeks following orchietomy. Testosterone, a male sex hormone with the highest concentration, can control the development and maintenance of masculine characteristics [11]. In a human epidemiological study, testosterone was demonstrated to be positively related to the BMD and fracture risk [12]. Separately, our μ CT examination showed that 4 weeks after castrating male rats, their bone volume decreased and the bone porosity increased. Accordingly, 1 month after orchietomy, bone loss similar to that in the early stage of osteoporosis had been induced. Furthermore, our tomographic and biomechanical data demonstrated decrements in the microarchitecture and strength of trabecular bone in orchietomized rats. In contrast, castration did not affect the tomographic or biomechanical characteristics of cortical bone. Our previous study demonstrated that a bilateral ovariectomy in rats lessened blood 17β -estradiol levels, the bone torsion force and bone mineral contents [27]. Vorland et al. reported that subsection of rats to ovariectomy led to a noteworthy loss of trabecular bone but did not affect cortical bone [37]. As the mechanism, the ovariectomy-induced estrogen deficiency induces bone loss due to a significant augmentation in osteoclast numbers [26]. In a male animal model of osteoporosis, orchietomy could augment bone turnover and triggered bone loss via activation of the RANKL-OPG signaling pathway [26, 29]. In men, loss of trabecular bone occurs much earlier than harm to cortical bone [8]. Herein, we present tomographic and biomechanical evidence to show specific loss of trabecular bone in the early stage of male osteoporosis.

Orchietomy interrupted the microarchitecture of trabecular bone. μ CT radiographic studies showed that 4 weeks after orchietomy in male Wistar rats, the volume of trabecular bone had diminished. The bone volume fraction can directly elucidate osteoporosis-induced variations in the assembly and strength of cancellous bone [38]. Subsequently, the porosity of cancellous bone increased following castration. In addition, our tomographic data displayed orchietomy-induced reduction in the trabecular bone number. A diminished trabecular bone number can clarify deterioration of the spongy bone microarchitecture and consequent existence of bone loss [39]. In addition, treatment of male Wistar rats with orchietomy decreased the separation of trabecular bone. Weinstein and Hutson stated that a reduction in the trabecular width was directly connected to bone loss with aging [34]. In comparison, the trabecular pattern factor was enhanced after orchietomy. The trabecular pattern factor is a histomorphometric parameter for informal quantification of the bone microarchitecture [40]. An increase in the value of the trabecular bone factor characterizes weaker trabecular connectivity [41].

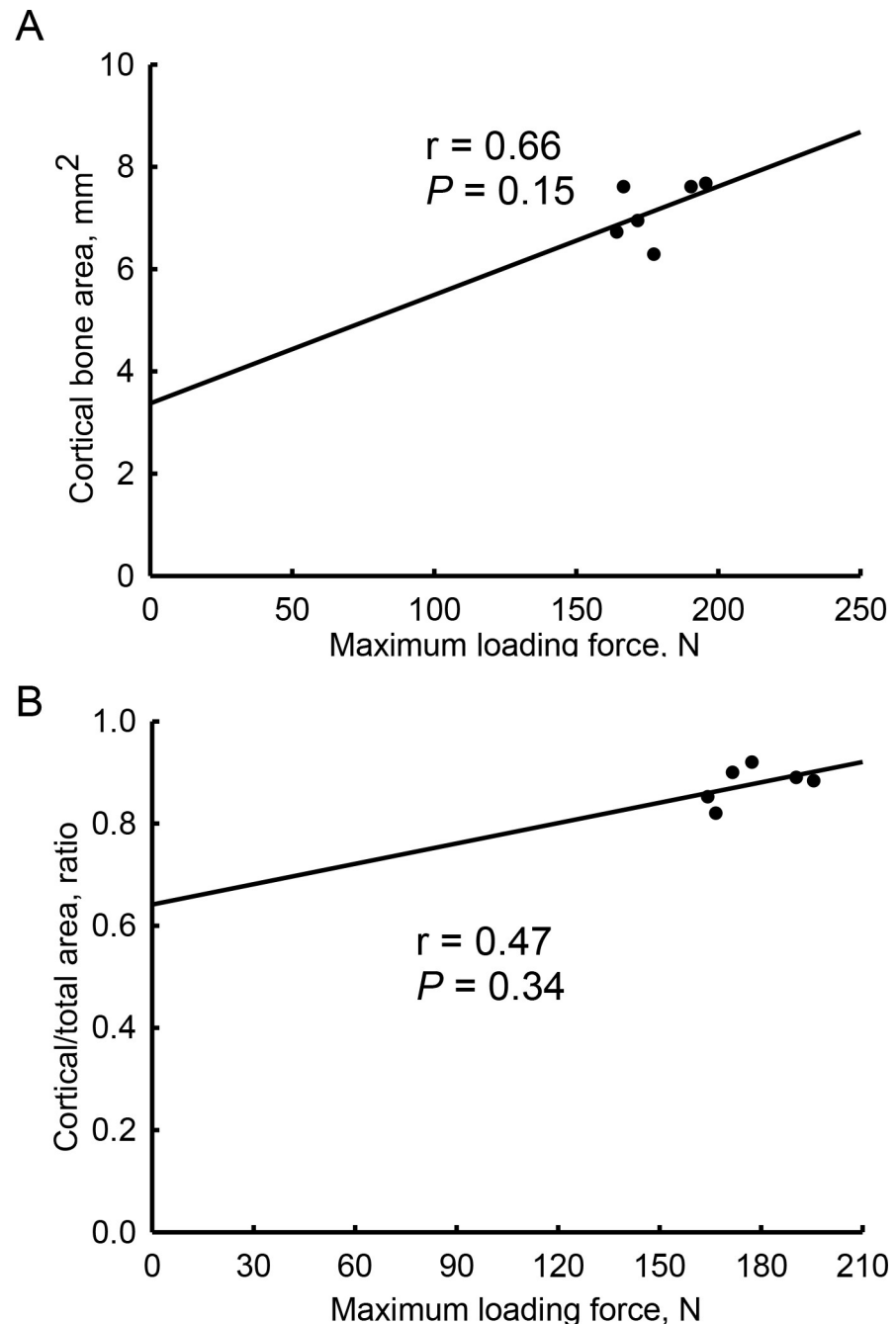


Fig 6. Associations of the biomechanical maximum loading force with tomographic parameters in orchietomy-treated cortical bone. Cortical bones from sham-operated and orchietomized rats were analyzed using micro-computed tomography and a reduced-platen compression test. The tomographic cortical bone area, ratio of cortical bone area over the total bone section area, and mechanical maximum loading force were measured. Correlations of the mechanical maximum loading force with the tomographic cortical bone area (A) and ratio of cortical bone area over total bone section area (B) were analyzed using linear regressions.

<https://doi.org/10.1371/journal.pone.0219718.g006>

Our previous study demonstrated the benefits of chitosan nanofiber scaffolds in reducing the trabecular bone factor value to improve bone healing [32]. Recently, we further showed a relationship of the trabecular bone factor with fracture healing [33]. A previous study reported

architectural changes in trabecular bone after rats had been castrated for 3~4 months [42]. Our current analyses of tomographic images and parameters disclosed the effects of orchietomy on altering the microarchitecture of trabecular bone in the primary phase of male osteoporosis.

Our biomechanical analysis additionally verified the orchietomy-induced reduction in the strength of trabecular bone. In this study, a reduced-platen compression test was applied to measure the strength of trabecular bone in tibias. This apparatus compresses the tibial specimen until a deforming point, which directly reflects the material resistance [34, 43]. After the orchietomy, the maximum loading force to break trabecular bone had significantly decreased. The displacement at the maximum load was also reduced in castrated rats. Moreover, the energy that was necessary to expand the maximum loading force to break a tibia decreased in castrated animals compared to the sham group. In a biomechanical test, decreases in the maximum loading force, displacement, and energy indicated a lessening of the strength of trabecular bone. Remarkably, the ultimate stress of trabecular bone in tibias declined following castration. The ultimate stress, also known as the compressive strength, is the capacity of bone to withstands loads [44]. A diminution in the ultimate stress of cancellous bone indicates orchietomy-induced weakening of the bone strength. More importantly, our biomechanical data representing the maximum loading force illustrated high correlations with the tomographic trabecular bone number, trabecular separation, and trabecular pattern factor in castrated rats. Previous studies reported that radiographic BMD cannot accurately reflect the osteoporosis-associated fracture risk [21–23]. Our present study additionally provides reliable compression data to support orchietomy-triggered disruptions in the microarchitecture and strength of trabecular bone in the early stage of male osteoporosis.

Orchietomy did not affect the microarchitecture or strength of cortical bone. Our radiographic data revealed that after castration, the thickness and bone area fraction of cortical bone in male Wistar rats were not influenced compared to sham animals. Our present findings are similar to the work of Blouin et al. who described how at 1 month after an orchietomy, the architecture of cortical bone in aged male Wistar rats had not changed [42]. Vandenput et al. showed a considerable difference in the volume of cortical bone 4 months after orchietomy in aged male Wistar Hannover rats [45]. Another study also revealed that long term (> 4 months) after orchietomy, the cortical bone mass was significantly affected [46]. In women, trabecular bone is lost with age [10]. In contrast, loss of cortical bone begins after the age of 75 years in men [8]. Nonetheless, loss of cortical bone in women occurs much earlier than in men [9]. In parallel, 4 weeks after orchietomy in male Wistar rats, the maximum loading force, displacement at the maximum load, bone stiffness, energy at the maximum load, and ultimate stress of cortical bone were not affected. Recently, Mohamad et al. reported that administration of rats with orchietomy for 3 months induced more bone loss in trabecular bone than in cortical bone [47]. In comparison, they conducted a three-point bending test but did not find any significant changes in biomechanical strength. Our biomechanical RPC and FPB analyses provide more lines of evidence to verify that compared to cortical bone, orchietomy can change the microarchitecture or strength of trabecular bone in the early stage of osteoporosis.

Conclusions

In summary, this study showed that 4 weeks after orchietomy in male Wistar rats, levels of testosterone in plasma significantly decreased which concurrently prompted bone loss. Our tomographic analyses revealed that orchietomy caused substantial alterations in the trabecular bone number, trabecular separation, and trabecular pattern factor. Fascinatingly, these orchietomy-induced tomographic differences in the microarchitecture of trabecular bone in

castrated rats were highly associated with biomechanical reductions in the maximum loading force, displacement at the maximum load, energy at the maximum load of trabecular bone. In contrast, there were no significant differences in the tomographic microarchitecture or biomechanical strength of cortical bone 4 weeks after orchietomy in Wistar rats. Taken together, the present study provides tomographic and biomechanical evidence to show specific insults to the microarchitecture and strength of trabecular bone in the early stage of male osteoporosis.

Supporting information

S1 Table. Raw data for Table 1.

(PDF)

S2 Table. Raw data for Table 2.

(PDF)

S1 Fig. Raw data for Fig 2.

(PDF)

S2 Fig. Raw data for Fig 3.

(PDF)

S3 Fig. Raw data for Fig 4.

(PDF)

Acknowledgments

The authors express their gratitude to Ms. Yi-Ling Lin for technical support and data collection during the experiments.

Author Contributions

Conceptualization: Poh-Shiow Yeh, Yuan-Wen Lee, Wei-Hui Chang, Jaw-Lin Wang, Ruei-Ming Chen.

Data curation: Poh-Shiow Yeh, Yuan-Wen Lee, Wei-Hui Chang, Weu Wang, Ruei-Ming Chen.

Formal analysis: Ruei-Ming Chen.

Funding acquisition: Ruei-Ming Chen.

Investigation: Poh-Shiow Yeh, Yuan-Wen Lee, Wei-Hui Chang, Weu Wang, Ruei-Ming Chen.

Methodology: Poh-Shiow Yeh, Yuan-Wen Lee, Wei-Hui Chang, Weu Wang, Jaw-Lin Wang, Ruei-Ming Chen.

Project administration: Ruei-Ming Chen.

Resources: Weu Wang, Jaw-Lin Wang, Shing-Hwa Liu, Ruei-Ming Chen.

Software: Yuan-Wen Lee, Wei-Hui Chang.

Supervision: Shing-Hwa Liu.

Validation: Yuan-Wen Lee, Jaw-Lin Wang, Shing-Hwa Liu, Ruei-Ming Chen.

Visualization: Ruei-Ming Chen.

Writing – original draft: Poh-Shiow Yeh, Yuan-Wen Lee, Wei-Hui Chang, Ruei-Ming Chen.

Writing – review & editing: Poh-Shiow Yeh, Yuan-Wen Lee, Wei-Hui Chang, Weu Wang, Jaw-Lin Wang, Shing-Hwa Liu, Ruei-Ming Chen.

References

1. Watts NB, GLOW investigators. Insights from the Global Longitudinal Study of Osteoporosis in Women (GLOW). *Nature Rev Endocrinol*. 2014; 10:412–22.
2. Gartlehner G, Patel SV, Feltner C, Weber RP, Long R, Mullican K, et al. Hormone therapy for the primary prevention of chronic conditions in postmenopausal women: evidence report and systematic review for the us preventive services task force. *JAMA*. 2017; 318:2234–49. <https://doi.org/10.1001/jama.2017.16952> PMID: 29234813
3. Raisz LG. Pathogenesis of osteoporosis: concepts, conflicts, and prospects. *J Clin Invest*. 2005; 115:3318–25. <https://doi.org/10.1172/JCI27071> PMID: 16322775
4. Lim SJ, Yeo I, Yoon PW, Yoo JJ, Rhyu KH, Han SB, et al. Incidence, risk factors, and fracture healing of atypical femoral fractures: a multicenter case-control study. *Osteoporos Int*. 2018; 29:2427–35. <https://doi.org/10.1007/s00198-018-4640-4> PMID: 30039251
5. Sidlauskas KM, Sutton EE, Biddle MA. Osteoporosis in men: epidemiology and treatment with denosumab. *Clin Interv Aging*. 2014; 9:593–601. <https://doi.org/10.2147/CIA.S51940> PMID: 24748777
6. Lee JH, Lee YK, Oh SH, Ahn J, Lee YE, Pyo JH, et al. A systematic review of diagnostic accuracy of vertebral fracture assessment (VFA) in postmenopausal women and elderly men. *Osteoporos Int*. 2016; 27:1691–9. <https://doi.org/10.1007/s00198-015-3436-z> PMID: 26782682
7. Viswanathan M, Reddy S, Berkman N, Cullen K, Middleton JC, Nicholson WK, et al. Screening to prevent osteoporotic fractures: updated evidence report and systematic review for the us preventive services task force. *JAMA*. 2018; 319:2532–51. <https://doi.org/10.1001/jama.2018.6537> PMID: 29946734
8. Riggs BL, Melton LJ, Robb RA, Camp JJ, Atkinson EJ, McDaniel L, et al. A population-based assessment of rates of bone loss at multiple skeletal sites: evidence for substantial trabecular bone loss in young adult women and men. *J Bone Miner Res*. 2008; 23:205–14. <https://doi.org/10.1359/JBMR.071020> PMID: 17937534
9. Wang J, Stein EM, Zhou B, Nishiyama KK, Yu YE, Shane E, et al. Deterioration of trabecular plate-rod and cortical microarchitecture and reduced bone stiffness at distal radius and tibia in postmenopausal women with vertebral fractures. *Bone*. 2016; 88:39–46. <https://doi.org/10.1016/j.bone.2016.04.003> PMID: 27083398
10. Aaron JE, Makins NB, Sagreya K. The microanatomy of trabecular bone loss in normal aging men and women. *Clin Orthop Relat Res*. 1987; 215:260–71.
11. Sinnesael M, Claessens F, Boonen S, Vanderschueren, D. Novel insights in the regulation and mechanism of androgen action on bone. *Curr Opin Endocrinol Diabetes Obes*. 2013; 20:240–4. <https://doi.org/10.1097/MED.0b013e32835f7d04> PMID: 23449008
12. Mohamad NV, Soelaiman IN, Chin KY. A concise review of testosterone and bone health. *Clin Interv Aging*. 2016; 11:1317–24. <https://doi.org/10.2147/CIA.S115472> PMID: 27703340
13. Nayak S, Greenspan SL. Osteoporosis treatment efficacy for men: a systematic review and meta-analysis. *J Am Geriatr Soc*. 2017; 65:490–5. <https://doi.org/10.1111/jgs.14668> PMID: 28304090
14. Almeida M, Laurent MR, Dubois V, Claessens F, O'Brien CA, Bouillon R, et al. Estrogens and Androgens in Skeletal Physiology and Pathophysiology. *Physiol Rev*. 2017; 97:135–87. <https://doi.org/10.1152/physrev.00033.2015> PMID: 27807202
15. Singh R, Artaza JN, Taylor WE, Braga M, Yuan X, Gonzalez-Cadavid NF, et al. Testosterone inhibits adipogenic differentiation in 3T3-L1 cells: nuclear translocation of androgen receptor complex with beta-catenin and T-cell factor 4 may bypass canonical Wnt signaling to down-regulate adipogenic transcription factors. *Endocrinology*. 2006; 147:141–54. <https://doi.org/10.1210/en.2004-1649> PMID: 16210377
16. Harman SM, Metter EJ, Tobin JD, Pearson J, Blackman MR. Longitudinal effects of aging on serum total and free testosterone levels in healthy men. *J Clin Endocrinol Metab*. 2001; 86:724–31. <https://doi.org/10.1210/jcem.86.2.7219> PMID: 11158037
17. Eastell R, Pigott T, Gossiel F, Naylor KE, Walsh JS, Peel NFA. Diagnosis of endocrine disease: bone turnover markers: are they clinically useful? *Eur J Endocrinol*. 2018; 178:R19–R31. <https://doi.org/10.1530/EJE-17-0585> PMID: 29046326

18. Jiang HX, Majumdar SR, Dick DA, Moreau M, Raso J, Otto DD, et al. Development and initial validation of a risk score for predicting in-hospital and 1-year mortality in patients with hip fractures. *J Bone Miner Res.* 2005; 20:494–500. <https://doi.org/10.1359/JBMR.041133> PMID: 15746995
19. Bliuc D, Nguyen ND, Milch VE, Nguyen TV, Eisman JA, Center JR. Mortality risk associated with low-trauma osteoporotic fracture and subsequent fracture in men and women. *JAMA.* 2009; 301:513–21. <https://doi.org/10.1001/jama.2009.50> PMID: 19190316
20. Kovacs CS. The skeleton is a storehouse of mineral that is plundered during lactation and (fully?) replenished afterwards. *J Bone Miner Res.* 2017; 32:676–80. <https://doi.org/10.1002/jbmr.3090> PMID: 28177150
21. Schmidt C, Priemel M, Kohler T. Precision and accuracy of peripheral quantitative computed tomography (pQCT) in the mouse skeleton compared with histology and microcomputed tomography (microCT). *J Bone Miner Res.* 2003; 18:1486–96. <https://doi.org/10.1359/jbmr.2003.18.8.1486> PMID: 12929938
22. Cefalu CA. Is bone mineral density predictive of fracture risk reduction? *Curr Med Res Opin.* 2004; 20:341–9. <https://doi.org/10.1185/030079903125003062> PMID: 15025843
23. Kanis JA, Johnell O, de Laet C. A meta-analysis of previous fracture and subsequent fracture risk. *Bone.* 2004; 35:375–82. <https://doi.org/10.1016/j.bone.2004.03.024> PMID: 15268886
24. Thomann M, Krause C, Angrisani N, Bormann D, Hassel T, Windhagen H, et al. Influence of a magnesium-fluoride coating of magnesium-based implants (MgCa0.8) on degradation in a rabbit model. *J Biomed Mater Res. A* 2010; 93:1609–19. <https://doi.org/10.1002/jbm.a.32639> PMID: 20073078
25. Jepsen KJ, Silva MJ, Vashishth D, Guo XE, van der Meulen MC. Establishing biomechanical mechanisms in mouse models: practical guidelines for systematically evaluating phenotypic changes in the diaphyses of long bones. *J Bone Miner Res.* 2015; 30:951–66. <https://doi.org/10.1002/jbmr.2539> PMID: 25917136
26. Almeida M, Laurent MR, Dubois V, Claessens F, O'Brien CA, Bouillon R, et al. Estrogens and androgens in skeletal physiology and pathophysiology. *Physiol Rev.* 2017; 97:135–87. <https://doi.org/10.1152/physrev.00033.2015> PMID: 27807202
27. Lee YE, Liu HC, Lin YL, Liu SH, Liao MS, Yang RS, Chen RM. *Drynaria fortunei* J. Sm. improves the bone mass of ovariectomized rats through osteocalcin-involved endochondral ossification. *J Ethnopharmacol.* 2014; 158: 98–104.
28. Chin KY, Gengatharan D, Mohd Nasru FS, Khairussam RA, Ern SL, Aminuddin SA, et al. The effects of annatto tocotrienol on bone biomechanical strength and bone calcium content in an animal model of osteoporosis due to testosterone deficiency. *Nutrients.* 2016; 8: pii: E808.
29. Jayusman PA, Mohamed IN, Alias E, Mohamed N, Shuid AN. The effects of quassinoid-rich *eurycoma longifolia* extract on bone turnover and histomorphometry indices in the androgen-deficient osteoporosis rat model. *Nutrients.* 2018; 10: pii: E799.
30. Wink CS, Felts WJ. Effects of castration on the bone structure of male rats: a model of osteoporosis. *Calcif Tissue Int.* 1980; 32:77–82. PMID: 6775783
31. Cauley JA, Burghardt AJ, Harrison SL, Cawthon PM, Schwartz AV, Connor EB, et al. (2018) Accelerated bone loss in older men: effects on bone microarchitecture and strength. *J Bone Miner Res.* 2018; 33:1859–69. <https://doi.org/10.1002/jbmr.3468> PMID: 29750848
32. Nazarian A, von Stechow D, Zurkowski D, Müller R, Snyder BD. Bone volume fraction explains the variation in strength and stiffness of cancellous bone affected by metastatic cancer and osteoporosis. *Calcif Tissue Int.* 2008; 83:368–79. <https://doi.org/10.1007/s00223-008-9174-x> PMID: 18946628
33. Rejnmark L, Sikjaer T, Underbjerg L, Mosekilde L. PTH replacement therapy of hypoparathyroidism. *Osteoporos Int.* 2013; 24:1529–36. <https://doi.org/10.1007/s00198-012-2230-4> PMID: 23184178
34. Weinstein RS, Hutson MS. Decreased trabecular width and increased trabecular spacing contribute to bone loss with aging. *Bone.* 1987; 8:137–42. PMID: 3606904
35. Hahn M, Vogel M, Pompesius-Kempa M, Delling G. Trabecular bone pattern factor—a new parameter for simple quantification of bone microarchitecture. *Bone.* 1992; 13:327–30. PMID: 1389573
36. Toben D, Schroeder I, El Khassawna T, Mehta M, Hoffmann JE, Frisch JT, et al. Fracture healing is accelerated in the absence of the adaptive immune system. *J Bone Miner Res.* 2011; 26:113–24. <https://doi.org/10.1002/jbmr.185> PMID: 20641004
37. Vorland CJ, Lachcik PJ, Swallow EA, Metzger CE, Allen MR, Chen NX, et al. Effect of ovariectomy on the progression of chronic kidney disease-mineral bone disorder (CKD-MBD) in female C57BL/6J rats. *Sci Rep.* 2019; 9:7936. <https://doi.org/10.1038/s41598-019-44415-9> PMID: 31138895
38. Liao MH, Lin PI, Ho WP, Chan WP, Chen TL, Chen RM. Participation of GATA-3 in regulation of bone healing through transcriptionally upregulating *bcl-xL* gene expression. *Exp Mol Med.* 2017; 49:e398. <https://doi.org/10.1038/emm.2017.182> PMID: 29170477

39. Blouin S, Gallois Y, Moreau MF, Basle MF, Chappard D. Disuse and orchidectomy have additional effects on bone loss in the aged male rat. *Osteoporos Int.* 2007; 18:85–92. <https://doi.org/10.1007/s00198-006-0197-8> PMID: 17019521
40. Swift JM, Gasier HG, Swift SN, Wiggs MP, Hogan HA, Fluckey JD, et al. Increased training loads do not magnify cancellous bone gains with rodent jump resistance exercise. *J Appl Physiol.* 1985; 109:1600–7.
41. Vahey JW, Lewis JL, Vanderby R. Elastic moduli, yield stress, and ultimate stress of cancellous bone in the canine proximal femur. *J Biomech.* 1987; 20:29–33. PMID: 3558426
42. Vandendput L, Boonen S, van Herck E, Swinnen JV, Bouillon R, Vanderschueren D. Evidence from the aged orchidectomized male rat model that 17beta-estradiol is a more effective bone-sparing and anabolic agent than 5alpha-dihydrotestosterone. *J Bone Miner Res.* 2002; 17:2080–6. <https://doi.org/10.1359/jbmr.2002.17.11.2080> PMID: 12412816
43. Vanderschueren D, van Herck E, Suiker AM, Visser WJ, Schot LP, Bouillon R. Bone and mineral metabolism in aged male rats: short and long term effects of androgen deficiency. *Endocrinology.* 1992; 130:2906–16. <https://doi.org/10.1210/endo.130.5.1572302> PMID: 1572302
44. Abdulai-Saiku S, Vyas A. Loss of predator aversion in female rats after *Toxoplasma gondii* infection is not dependent on ovarian steroids. *Brain Behav Immun.* 2017; 65:95–8. <https://doi.org/10.1016/j.bbi.2017.04.005> PMID: 28400143
45. Savaridas T, Wallace RJ, Dawson S, Simpson AH. Effect of ibandronate on bending strength and toughness of rodent cortical bone: Possible implications for fracture prevention. *Bone Joint Res.* 2015; 4:99–104. <https://doi.org/10.1302/2046-3758.46.2000311> PMID: 26062566
46. Keller TS, Mao Z, Spengler DM. Young's modulus, bending strength, and tissue physical properties of human compact bone. *J Orthop Res.* 1990; 8:592–603. <https://doi.org/10.1002/jor.1100080416> PMID: 2355299
47. Mohamad NV, Che Zulkepli MAA, May Theseira K, Zulkifli N, Shahrom NQ, Ridzuan NAM, et al. Establishing an animal model of secondary osteoporosis by using a gonadotropin-releasing hormone agonist. *Int J Med Sci.* 2018; 15:300–8. <https://doi.org/10.7150/ijms.22732> PMID: 29511366